Ultramicroscopy 185 (2018) 21–26

Contents lists available at ScienceDirect

Ultramicroscopy

journal homepage: www.elsevier.com/locate/ultramic

In-situ elastic strain mapping during micromechanical testing using EBSD

Mark J. McLean*, William A. Osborn

Materials Measurement Science Division, National Institute of Standards and Technology, United States

ARTICLE INFO

Article history:
Received 9 June 2017
Revised 2 November 2017
Accepted 13 November 2017
Available online 14 November 2017

ABSTRACT

Compared to more commonly used strain measurement techniques, electron backscatter diffraction (EBSD) offers improved spatial resolution and measurement sensitivity. Additionally, EBSD can provide the full deformation tensor, whereas other techniques, such as digital image correlation (DIC), are limited to only in-plane strains and rotations. In this work, EBSD was used to measure strains and rotations *in-situ* during testing of a single-crystal silicon micromechanical test specimen. The theta-like specimen geometry was chosen due to the complex and spatially-varying strain states that exist in the circular frame of the sample during testing, as well as the nominally uniform strains in the central web. Full-field strain maps were generated for each strain and rotation component and compared to those from finite element analyses (FEA), showing strong agreement in all cases. Additionally, potential sources of error and their impact on both measurement accuracy and uncertainty are discussed.

Published by Elsevier B.V.

1. Introduction

In-situ observation of micromechanical tests has become increasingly common, particularly through the development of electron microscope-compatible mechanical testing platforms. This capability allows for direct measurement of strain during the test, and a number of techniques have been developed for doing so [1]. For tests conducted in a scanning electron microscope (SEM), the most commonly used of these techniques is digital image correlation (DIC), where the location of individual features on the surface of the sample are tracked throughout the test and strain maps are generated based on the relative displacements between these markers [2]. In the SEM environment, this technique is limited to two dimensions, meaning that only the in-plane components of the deformation tensor can be measured. There are other techniques available that can also operate at this size scale, including Raman microscopy [3], X-ray diffraction [4], and a handful of others. However, these techniques all come with their own limitations and complications.

There is an SEM-based technique that can measure the full 3-D deformation tensor: electron backscatter diffraction (EBSD). Commonly referred to as the Wilkinson method, this technique involves capturing EBSD patterns from multiple locations on the sample, typically in a line scan or rectangular map, and then analyzing differences between the patterns to calculate the relative deformations between them [5,6]. This cross-correlation process is similar to the feature tracking involved in 2-D DIC; however, because EBSD patterns are representative of reciprocal space and not the actual specimen surface, it is possible to extract 3-D information. This means that the entire deformation tensor, including out-of-plane strains and rotations can be determined.

The Wilkinson method has been successfully used to measure strains in epilayer films, typically SiGe on Si, where the strain state in the film is simple and well-defined [6,7]. More complex strain states have been measured *ex-situ* in the vicinity of indents and cracks in Si and Ge, and shown good agreement with other techniques and expected values [3,8].

In more recent years, EBSD has been utilized to measure strains and rotations *in-situ* during various types of mechanical tests. These include four-point bending of single-crystal Si [7], uniaxial tension of steel [9], micropillar compression of GaAs [10,11] and Ti [12], and micro-cantilever bending in single-crystal W [13]. These works all show that EBSD can be used to measure strains *in-situ* while an external mechanical load is applied to the sample. The work presented here will extend this concept to a micromechanical specimen with a much more complicated geometry, leading to more complex and spatially-varying strain states in some areas. Additionally, an area of the sample expected to have a uniform strain state will be used to address both the accuracy and uncertainty of *in-situ* EBSD strain measurements.

* Corresponding author.
E-mail address: mark.mclean@nist.gov (M.J. McLean).

https://doi.org/10.1016/j.ultramic.2017.11.007
0304-3991/Published by Elsevier B.V.

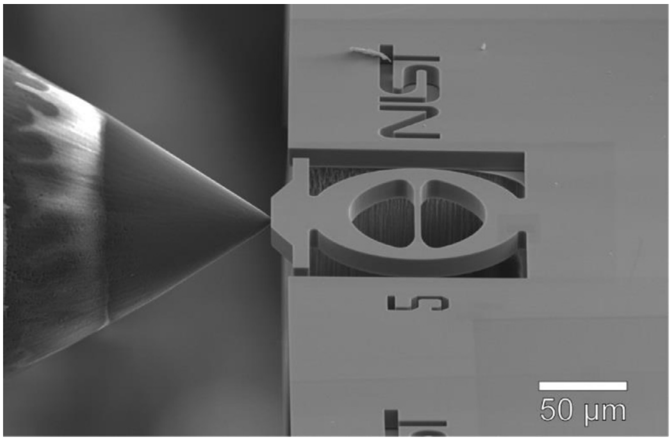

Fig. 1. SEM image showing indenter tip in contact with theta specimen. Image taken at 65° stage tilt.

2. Experiment

2.1. Specimen design and fabrication

The design and fabrication of the theta-like specimens used here has been described in detail previously [14]. In short, specimens were fabricated from silicon-on-insulator (SOI) wafers using standard microfabrication processes. In this specimen, the central web is the primary area of interest and was designed to have a width of 8 μm. For the individual sample used in this work, this web width was measured to be 6.9 μm. This offset is caused by a combination of lithography biases and etching undercuts. Additionally, the sample thickness was measured to be 24.1 μm. These measured dimensions were used in all subsequent analyses and models.

2.2. In-situ EBSD measurements

The *in-situ* EBSD experiments were conducted in a JEOL 7SM7100 FE-SEM equipped with an Oxford NordlysNano EBSD detector. An accelerating voltage of 20 kV was used with a probe current of 3.2 nA. A 150 mN load was applied to the sample using a Hysitron PI85xR indentation system in load control mode with a conospherical tip featuring a 5 μm tip radius. The system was oriented such that the indentation axis was parallel to the axis of stage tilt. The SEM stage was tilted to 65° with a working distance of 13.5 mm, which allowed the EBSD detector to be fully inserted into the chamber. Fig. 1 shows an SEM image taken with the indenter tip in contact with the specimen. It should be noted that although this image was taken with a dynamic focus correction to ensure a totally in-focus image despite the large specimen tilt, this feature was turned off for all EBSD data collection, as the image distortions it causes at low magnifications were problematic for calculating strains and rotations.

Two different EBSD maps were collected. The first was 400 μm × 385 μm with a 1.5 μm step size, encompassing the entire theta specimen as well as some of the surrounding material. This data set was used for all strain and rotation calculations. The second map was 370 μm × 390 μm with a 10 μm step size taken from the unstrained Si away from the theta specimen. This second data set was used for calculating the effective EBSD camera pixel size and actual specimen tilt, both of which are required inputs for calculating strains and rotations at each data point in the map. After testing, the sample was removed from the indentation system so that the contact surface could be imaged in the SEM. From these images, both the specimen thickness and location of the contact point were determined. This location was used in the subsequent FEA analyses.

2.3. In-situ confocal measurements

To provide an additional check on the out-of-plane rotations measured by EBSD, the same *in-situ* experiment described above was carried out under a Zeiss LSM800 confocal microscope. This measurement provided the vertical position at each point on the sample, from which the out-of-plane rotations could be determined by calculating the surface normal. This technique is not capable of providing any information regarding strains or in-plane rotations. Thus, it was simply used as an additional check on the out-of-plane rotation.

2.4. Strain and rotation calculations

The commercial software package, CrossCourt3 [15], was used to calculate the strain and rotation components from the EBSD maps. For the cross-correlation process, 37 regions of interest (ROIs), each 256 pixels by 256 pixels in size, were arranged in two concentric circles about the intensity center of the backscatter pattern (EBSP). ROIs of this size have been shown to produce strain and rotation measurements with the highest precision [6], and the annular distribution provides uniform coverage in all directions with limited overlap, which increases computation time without improving the measurement precision.

Furthermore, to ensure that only data points truly on the top surface of the sample were included, a mask based on the pattern quality was applied to ensure that only high-quality patterns were being used. Additionally, a 1 pixel erosion was applied universally to the masked data set to exclude data points on corners or sidewalls of the sample. With the data set finalized in this state, all the strain and rotation data could be analyzed and plotted.

The data from the unstrained Si map was also analyzed using the same software; however, for this data the reference pattern was chosen as the center point in the map and a single ROI was placed at the pattern center. This ROI location is critical for this application as it makes the X- and Y-pattern shifts due to beam motion independent of one another.

2.5. Finite element analysis

The commercial software package, Abaqus, was used to perform FEA simulations for comparison with the experimental strains and rotations. The modeling procedure used here was similar to that described elsewhere [16], with a few notable differences. In short, quadratic tetrahedral elements were used in conjunction with an iterative mesh refinement algorithm based on the Mises stress error indicator to ensure convergence. Additionally, a skin of shell elements with effectively zero thickness and stiffness was added to the top surface of the model to allow rotations to be extracted, matching the crystal rotations measured experimentally.

The contact between the indenter tip and the sample was simulated by applying a surface traction along a specified vector almost normal to the surface to a circular region with a radius of 1.5 μm. Additionally, the magnitude of the surface traction was spatially varied radially with a Gaussian form to more closely resemble sphere on plane contact. This approach allows an angular misalignment between the tip and specimen to be modeled. Because this angle cannot be accurately measured, it was determined by fitting the FEA data to the experimental data. To do this, the angular misalignment was varied until the ω_2 value at the outer edge of the top hat matched the experimental value at the same location. This location was chosen as it should be essentially strain-free

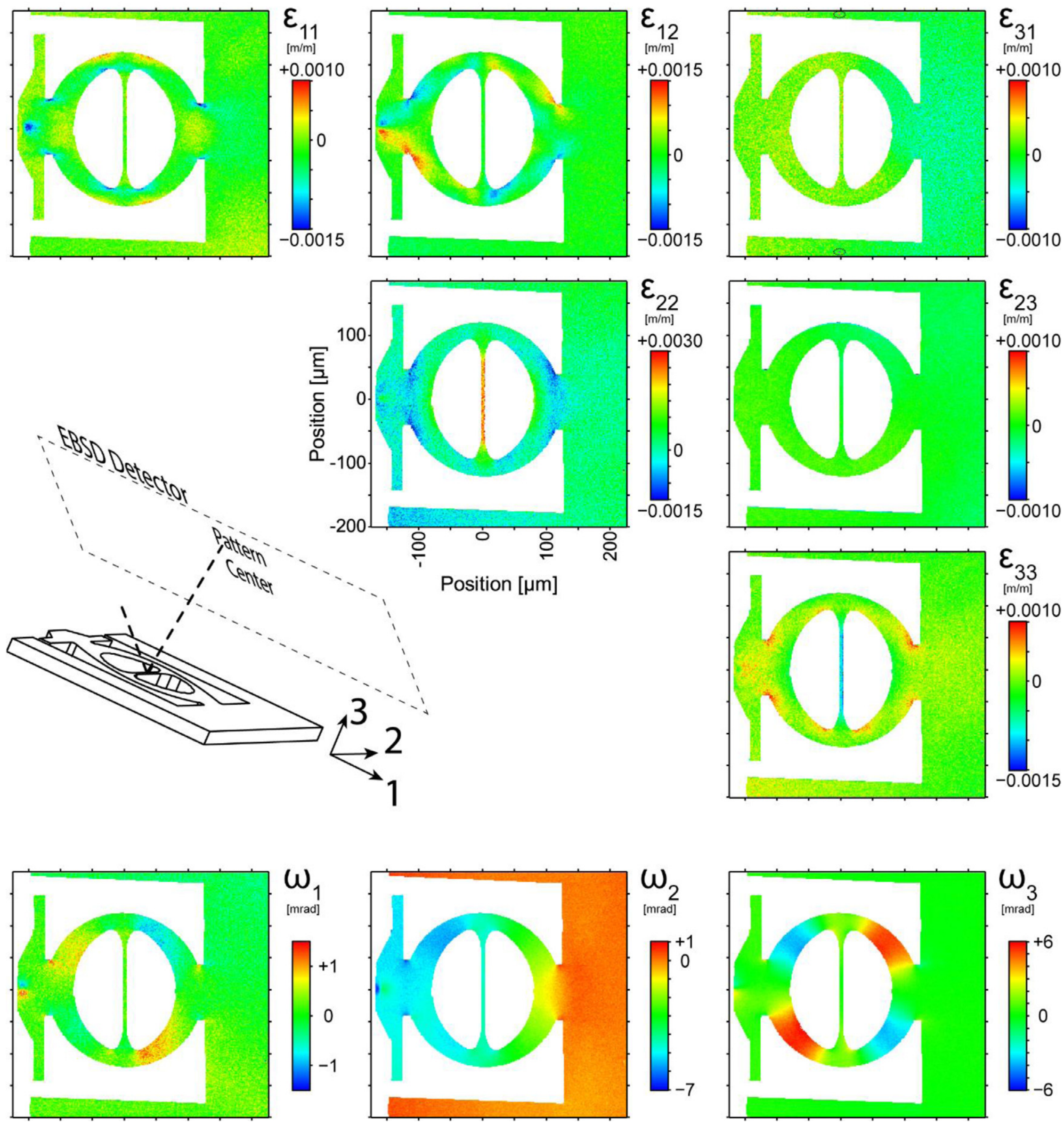

Fig. 2. Strain and rotation maps for each component measured in-situ using cross-correlative EBSD. The locations of reference points are identified by the small black circles at the top and bottom of the ε_{31} map.

and the other rotation components should be minimal. An angular misalignment of 1.1° out of plane away from the surface normal of the top surface of the sample was determined and used in all subsequent modeling.

3. Results and discussion

3.1. Calculation of effective pixel size and specimen tilt angle

The mechanical complexity of the *in-situ* experiment requires many additional degrees of displacement and rotational freedom be introduced when compared to EBSD on a static sample. Because the magnitude of the sample tilt determines the relationship between vertical EBSP shift and electron beam motion, a procedure for finding sample tilt empirically is required. The EBSD map from the unstrained silicon sample is well suited for determining both effective pixel size and specimen tilt simultaneously.

Although the camera pixels on the EBSD detector are square and have a defined physical size, microscope calibration and detector lenses allow the effective pixel size to be different from the physical pixel size. A map collected with identical microscope conditions from an unstrained region of the sample should yield shifts in the EBSP caused only by beam motion. Analyzing this map cross-correlation with a single ROI located at the pattern center separates the x- and y-components of the beam motion induced pattern shifts. The x-component of shift is fit with respect to x-motion of the beam to determine an effective pixel size for the detector and microscope calibration. Because the camera pixels of the EBSD detector are known to be square, the y-components of shift can be fit with respect to sample tilt using the effective pixel size from the x-direction. For this dataset, the effective pixel size and sample tilt were determined to be 24.0 μm and 65.2°, respectively. This effective pixel size is very close to the camera pixel size of the EBSD detector, indicating the product of the EBSD detector's

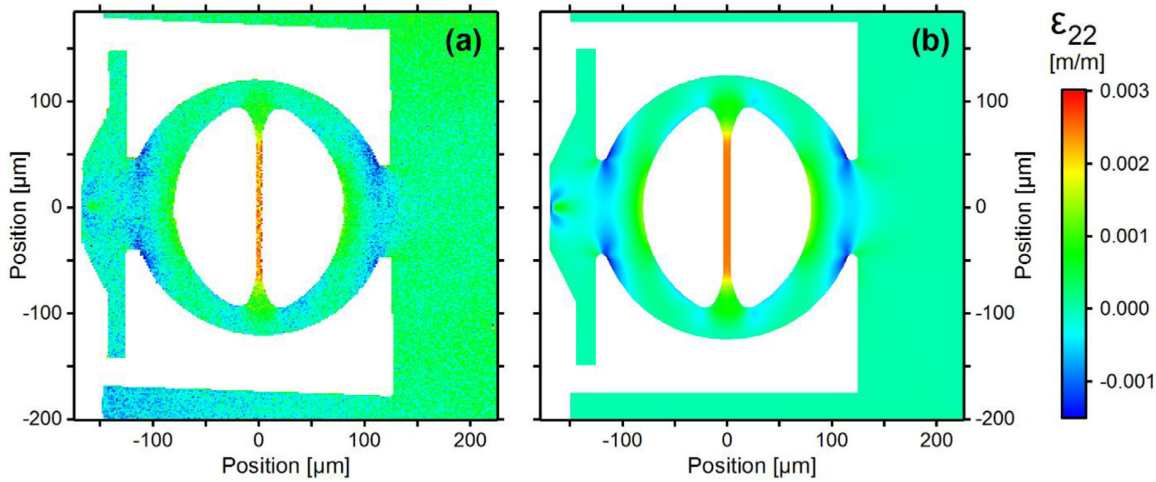

Fig. 3. Comparison of (a) EBSD and (b) FEA strain maps for ε_{22}.

lens magnification (nominally 1.0×) and the microscope's magnification calibration error factor (ideally 1.0×) is near 1.0.

3.2. In-situ elastic strain and rotation mapping

Using the effective pixel size and sample tilt from 3.1, cross-correlation strain measurement was performed with four different nominally deformation-free reference points. These points were located in the unstrained frame surrounding the sample and vertically aligned with the central web. Two points were chosen from the top of the map and two from the bottom. Multiple reference points were chosen to minimize the effect of any beam-positioning errors introduced by the SEM, which would lead to gradients in several of the calculated strain and rotation components. The strains and rotations at each point in the map from the different reference points were averaged together and the resulting maps are shown in Fig. 2. The exact locations of the reference points are identified as well.

There are several important aspects of these strain maps. First, because the stress state in the central web of the theta is known to be uniaxial tension, the strain state in the web is correctly measured to have a large positive value parallel to this direction (ε_{22}), smaller negative values in the orthogonal directions due to Poisson contraction (ε_{11} and ε_{33}), and near-zero values for the shear components. Second, outside the web region complex strain states are observed, including stress intensification near filleted corners and complex rotations and shears in the top-hat region where the indenter contacts the theta structure. Third, there is a very clear out-of-plane rotation, ω_2, showing that the specimen had deflected down (away from the top surface of the wafer) during the test. This bending behavior is caused by small misalignments between the indentation axis and the specimen midplane. This will be discussed in more detail in the following section. Next, although there are some gradients measured in the perimeter structure that is assumed to be strain- and rotation-free, the magnitude is only marginally larger than the noise level, and thus is not a major concern. Finally, the theta and its rectangular perimeter exhibit a slight skew, as evidenced by the corners at top and bottom of the map having non-right angles. The most likely cause of this is image distortion in the SEM that is difficult to avoid at low magnifications. Since the electron beam position must be precisely known to separate the beam motion and strain induced shifts of an ROI, small errors in beam placement (SEM image distortion) may also contribute to the otherwise anomalous gradients mentioned above [7].

3.3. Comparison with FEA

In addition to demonstrating the versatility of using EBSD to measure strain during in-situ experiments, a goal of this work is to establish the accuracy and uncertainty of strains measured during such experiments. The theta structure has been used previously because applied load can be used in conjunction with FEA to predict the uniaxial stress in the web. With the experimental setup in this work, the load can be set and strain on the front surface of the device can be measured everywhere, which should match FEA results. Since the strain in the web, ε_{22}, is directly related to the primary figure of merit for the theta structure (the tensile stress in the web), the EBSD and FEA results from ε_{22} are presented in Fig. 3:

Comparing these two maps shows that location and spatial extent of the strain features matches extremely well. The largest strain magnitude is in the web, with compressive regions at the connection between the top-hat and base, as well as additional features near the indenter contact site and where the web joins the ring. Similar agreement is found between the EBSD and FEA results on the other 8 strain and rotation components and is shown in full in Fig. S1 in the supplemental info. To assess the agreement in a more quantitative fashion, the EBSD and FEA values were extracted on a line along the central web of the sample. This data is presented in Fig. 4.

For this data set, there were four columns worth of pixels from the EBSD map contained within the gauge section of the central web. These four values have been averaged for each map row to form the data presented in Fig. 4, with the shaded envelope representing the min-max range for each map row. This presentation allows visual interpretation of both the accuracy and uncertainty of the measurement. From this plot, the strong agreement between the measured and expected values of ε_{22} and ε_{33} can be clearly observed. This holds true not only in the gauge section, where the values are nominally uniform, but also outside the web in the outer frame of the sample where more complex strain gradients exist. The average value of each individual component, along with its uncertainty, defined as one standard deviation (1σ), over the entire gauge section is summarized in Table 1.

The agreement between simulation and experiment is good with the expected value from FEA falling within 1σ of the EBSD-measured value for most components. Additionally, the strain sensitivity from EBSD measurements, typically defined as the standard deviation of a set of nominally uniform measurements, has been previously determined to be approximately 2×10^{-4} [5,6,8], which

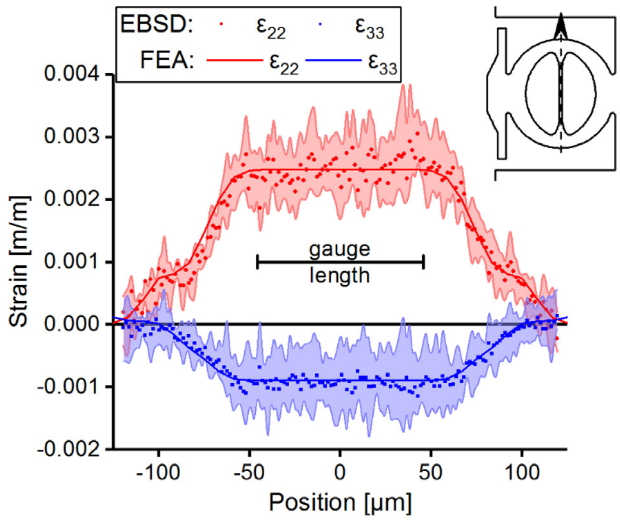

Fig. 4. Line scans of ε_{22} and ε_{33} strains extracted from full field maps. The path of the line runs along the central web. For the EBSD data, the individual data points represent the mean strain value for each horizontal row, containing 4 EBSD map points. The shaded region represents the min/max envelope for each row as well.

Table 1
Strain and rotation values in the gauge length of the central web of theta specimen. EBSD values are reported as the mean ± one standard deviation (1σ).

		FEA	EBSD
ε_{11}	[m/m × 10^{-3}]	−0.15	−0.07 ± 0.21
ε_{22}		2.48	2.49 ± 0.48
ε_{33}		−0.90	−0.94 ± 0.23
ε_{12}		0.00	−0.03 ± 0.17
ε_{23}		0.00	−0.07 ± 0.10
ε_{31}		0.00	0.30 ± 0.20
ω_1	[mrad]	0.00	0.36 ± 0.28
ω_2		−4.78	−4.47 ± 0.18
ω_3		0.01	0.19 ± 0.24

also agrees with the uncertainty measured here. For those values where the expected value does not fall within 1σ of the measured value, or the uncertainty is larger than expected, there are two potential sources of error.

The first is the observed image distortion discussed previously. Accurate calculation of strain and rotation components requires accurate knowledge of the beam position, and image distortion introduces error in beam position that is unaccounted for. The second is that the overall pattern quality observed during the *in-situ* experiments was noticeably reduced when compared to typical EBSD patterns from solid Si wafers, as shown in Fig. S2 in the supplemental information. Both of these issues could reduce accuracy and increase uncertainty in the calculation of EBSD pattern shifts.

As shown in Fig. 2 and Table 1, the EBSD results show a large (5 mrad) rotation of the theta out of plane around the 2 direction, ω_2. In a perfectly ideal experiment, the contact between the indenter and sample occurs exactly in the center of the thickness and is exactly normal to the surface. This ideal case should result in essentially zero out-of-plane rotations. However, given the large number of mechanical degrees of freedom, a small misalignment (both spatial and angular) between the indenter axis and the neutral axis of the theta is not surprising. As previously mentioned, the spatial and angular misses from ideal for this experiment were determined to be 2 μm and 1.1°, respectively, and these values were incorporated into the FEA models. Thus, for this rotation, the FEA alone is not sufficient to validate the experimental values, making the *in*-situ confocal measurements necessary. Confocal microscopy provides the surface height at a given location, from which the surface normal can be determined by fitting a local plane. Maps of this displacement from confocal and FEA can be seen in Fig. S3 in the supplemental information. The rotation is then simply the deviation of the measured surface normal from vertical. It should be noted that both ω_1 and ω_2 can be measured this way, but ω_1 is very small and of little consequence for this sample geometry. The maps of ω_2 from all three techniques are shown in Fig. 5.

As stated above, since the FEA model was set up so that the ω_2 rotation matched the experiment, the agreement between those maps should be expected. However, the confocal map is an independent measurement and shows strong agreement, both in the spatial distribution of gradients and in the overall magnitude of the rotation. To further quantify this agreement, a line scan from the indentation location through the center of the theta base is provided in Fig. 6.

Again, this plot shows good agreement between all three techniques. It is important to remember that this out-of-plane rotation is not measurable by most techniques, such as DIC or Raman microscopy. And while confocal microscopy can provide this information, it cannot be used to measure strains of any kind, or in-plane rotations for that matter, on its own. Thus, the ability to measure the full deformation tensor from EBSD provided the insight necessary to determine the experimental misalignment responsible for observable differences between the ideal and real-life experiments. This is important because sample alignment in nano- and micro-scale mechanical tests is not trivial and even *in-situ* experiments often lack the depth perception required to be able to visualize this alignment in 3-D. Without a direct measurement of the out-of-plane deformation, one would have to rely on the measured compliance and/or shape of the load-displacement curve to determine if the sample was properly aligned and if any undesired bending moments were being applied during the test.

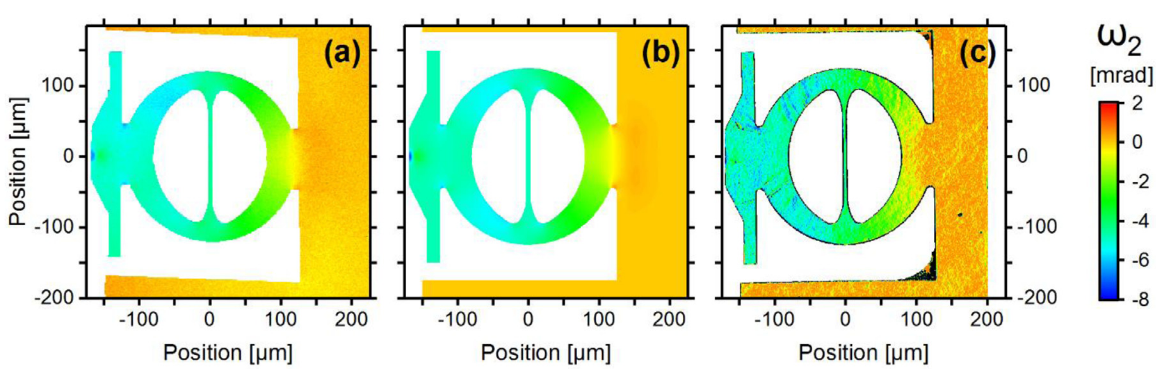

Fig. 5. Maps of ω_2 from (a) EBSD, (b) FEA, and (c) confocal microscopy. The negative rotation values mean that the sample is deflecting below the plane of the surface.

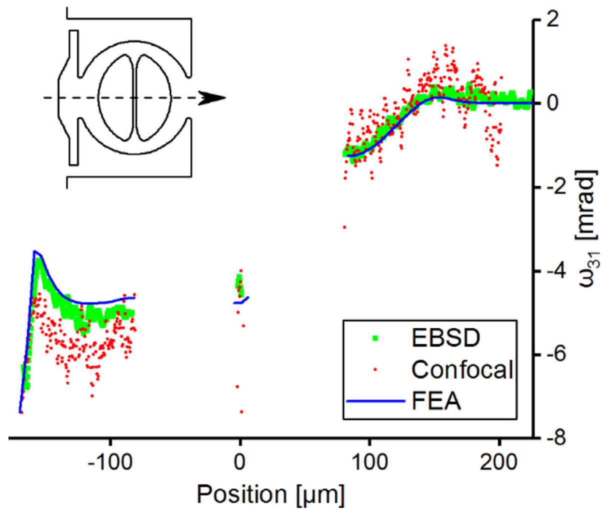

Fig. 6. Line scans of ω_2 extracted from EBSD, FEA, and confocal microscopy. Path of line is parallel to indentation axis, and shows the out-of-plane deflection caused by small misalignment with sample.

4. Conclusions

(1) Wilkinson-style EBSD strain analysis has been used to map strains and rotations *in-situ* during micromechanical testing of a single-crystal Si sample. Measured strains and rotations showed excellent qualitative and quantitative agreement with those predicted from FEA simulations.
(2) In the gauge section of the sample, where the stress state is known to be uniaxial tension and the only rotation is out-of-plane due to misalignment with the indenter, most of the strain and rotation components were measured to be within one standard deviation (1σ) of the expected value from FEA. Additionally, the uncertainties for each component were comparable to previously published values of measurement sensitivity. Any observed inaccuracies or increased uncertainty are likely due to either image distortion in the SEM or reduced EBSD pattern quality compared to typical EBSD measurements.
(3) The out-of-plane rotation caused by small misalignments between the sample and the indenter tip was measured by EBSD (and verified by confocal microscopy). For small-scale mechanical tests, these small misalignments are very difficult to avoid and nearly impossible to measure directly. Combined with the FEA modeling, these measurements allowed the misalignments to be quantified in a way that most other *in-situ* strain measurement techniques, which provide only 2-D information, could not provide. This clearly illustrates one of the primary advantages of EBSD over other techniques.
(4) The ability to accurately measure strains and rotations in specimens at this size scale suggests that it is possible to measure them in real-world devices of a similar size. If a microelectromechanical system (MEMS) device has a complex geometry where large strain gradients are present during use, an *in-situ* measurement could allow these strains to be mapped directly, rather than relying solely on FEA. This could be especially important for the out-of-plane components, as MEMS devices often have tight clearances underneath moving components, or rely heavily on small vertical displacements for their operation. *In-situ* EBSD measurements would allow these out-of-plane strains and rotations to be measured directly.

Disclaimer

Any mention of commercial products is for informational purposes only and does not imply recommendation or endorsement by the National Institute of Standards and Technology.

Supplementary materials

Supplementary material associated with this article can be found, in the online version, at doi:10.1016/j.ultramic.2017.11.007.

References

[1] M. Legros, D. s. Gianola, C. Motz, Quantitative in situ mechanical testing in electron microscopes, MRS Bull. 35 (05) (2010) 354–360.
[2] B. Pan, K. Qian, H. Xie, A. Asundi, Two-dimensional digital image correlation for in-plane displacement and strain measurement: a review, Meas. Sci. Technol. 20 (2009).
[3] M.D. Vaudin, Y.B. Gerbig, S.J. Stranick, R.F. Cook, Comparison of nanoscale measurements of strain and stress using electron back scattered diffraction and confocal Raman microscopy, Appl. Phys. Lett. 93 (2008) 193116.
[4] D. Kiener, W. Grosinger, G. Dehm, R. Pippan, A further step towards an understanding of size-dependent crystal plasticity: in situ tension experiments of miniaturized single-crystal copper samples, Acta Mater 56 (3) (2008) 580–592.
[5] A.J. Wilkinson, Measurement of elastic strains and small lattice rotations using electron back scatter diffraction, Ultramicroscopy 62 (1996) 237–247.
[6] A.J. Wilkinson, G. Meaden, D.J. Dingley, High-resolution elastic strain measurement from electron backscatter diffraction patterns: new levels of sensitivity, Ultramicroscopy 106 (March(4–5)) (2006) 307–313.
[7] S. Villert, C. Maurice, C. Wyon, R. Fortunier, Accuracy assessment of elastic strain measurement by EBSD, J. Microsc. 223 (2) (2009) 290–301.
[8] B. Britton, I. Holton, G. Meaden, D. Dingley, High angular resolution electron backscatter diffraction: measurement of strain in functional and structural materials, Microsc. Anal. 27 (4) (2013) 8–13.
[9] M. Ojima, Y. Adachi, S. Suzuki, Y. Tomota, Stress partitioning behavior in an fcc alloy evaluated by the in situ/ex situ EBSD-Wilkinson method, Acta Mater. 59 (2011) 4177–4185.
[10] C. Niederberger, W.M. Mook, X. Maeder, J. Michler, In situ electron backscatter diffraction (EBSD) during the compression of micropillars, Mater. Sci. Eng. A 527 (2010) 4306–4311.
[11] X. Maeder, W.M. Mook, C. Niederberger, J. Michler, Quantitative stress/strain mapping during micropillar compression, Philos. Mag. 91 (7–9) (2011) 1097–1107.
[12] Y. Guo, J. Schwiedrzik, J. Michler, X. Maeder, On the nucleation and growth of {1122} twin in commercial purity titanium: In situ investigation of the local stress field and dislocation density distribution, Acta Mater. 120 (2016) 292–301.
[13] J. Ast, G. Mohanty, Y. Guo, J. Michler, X. Maeder, In situ micromechanical testing of tungsten micro-cantilevers using HR-EBSD for the assessment of deformation evolution, Mater. Des. 117 (2017) 265–266.
[14] M.S. Gaither, F.W. DelRio, R.S. Gates, R.F. Cook, Deformation and fracture of single-crystal silicon theta-like specimens, J. Mater. Res. 26 (20) (2011) 2575–2589.
[15] *CrossCourt3*. BLG.
[16] R. Kirkpatrick, W.A. Osborn, M.S. Gaither, R.S. Gates, F.W. DelRio, R.F. Cook, On the bending strength of single-crystal silicon theta-like specimens, MRS Commun. 3 (02) (2013) 113–117.